Analysis of the forward and reverse bias I-V and C-V characteristics on Al/PVA:n-PbSe polymer nanocomposites Schottky diode

S. K. Tripathi[a] and Mamta Sharma
Department of Physics, Center of Advanced Study in Physics, Panjab University, Chandigarh-160 014, India

(Received 7 November 2011; accepted 27 February 2012; published online 10 April 2012)

This paper presents the fabrication and characterization of the Al/PVA:n-PbSe Schottky diode. I-V characteristics have been measured at different temperatures in the forward bias. The behavior study of the series resistance (R_S), the ideality factor (n), the effective barrier height (Φ_b), the Richardson constant (A*), and the leakage current with the temperature have emphasized an inhomogeneity of the barrier height and a tunneling mechanism assisted by traps in the SBD. In C-V measurements, in the reverse bias, the Al/PVA:n-PbSe has been performed as a function of temperature and frequency. The values of barrier height ($\Phi_{C\text{-}V}$), the built-in–voltage (V_{bi}) and carrier concentration (N_D) and depletion layer width (W) have been calculated at different temperatures in reverse bias. The barrier inhomogeneities of the Al/PVA:n-PbSe contact has been explained on an assumption of a Gaussian distribution of barrier heights by using the potential fluctuation model. © *2012 American Institute of Physics*. [http://dx.doi.org/10.1063/1.3698773]

I. INTRODUCTION

Nanoparticles (NPs) with polymer fillers relate to the strong current interest in development and application of new materials called polymer nanocomposites.[1,2] These polymer nanocomposites have long-term stability and reprocesses ability. It serves to limit particle growth and stabilize nanocrystals. Polymer–inorganic nanocomposites have attracted much attention recently due to their unique size-dependent chemical and physical properties. Most researches have been done in II-VI or III-V semiconductors. Compared to these materials, IV-VI semiconductors, such as PbSe have larger exciton Bohr radius (~46 nm) and narrow bandgap semiconductor ($E_g \sim 0.27$ eV).[3] PbSe quantum dots are considered as large strong-confinement effect, which cannot be accessed in other materials. PbSe is a very attractive semiconductor material due to its wide variety of applications in photovoltaic absorbers, IR detectors, photographic and memory-switching devices,[4–6] thermoelectric cooling materials, laser materials, optical sensors, supersonic materials, optical recording materials, and solar cells.[7–10] Polyvinyl alcohol (PVA) is chosen as the polymer matrix for its aqueous solubility. The high viscosity of the polymer solution would be helpful in controlling the growth of selenide nanocrystals. Furthermore, from the application point of view, the polymer matrix would protect the selenide particles against photo oxidation. Normally PVA is a poor electrical conductor, and the conductivity of the polymer is of major importance in constructing a Schottky barrier. Its electrical conductivity depends on the thermally generated carriers and the addition of suitable dopant materials. When a polymer is doped with semiconductor, especially the II-VI semiconductor, such as PbSe, ZnSe, and CdSe in various quantities and forms, their incorporation within a polymeric system may be expected to improve the conductivity.[11,12] In other words, diffusion of the dopant material into polymer matrix plays an important role in the conduction process. The doping process affects the chemical structure, crystallinity, and electrical conductivity of polymers.[13] A low doping of the polymer associated with a low number of charge carriers can lead to an extended depletion layer in the structure. On the other hand, high-charge carrier densities in the polymer may give rise to a thin barrier with a high probability of tunneling through the barrier.

Therefore in the present study, the lead selenide doped PVA (PVA:n-PbSe) interfacial layer has been formed onto the front surface of Al substrate. However, the formation of the Schottky barrier at the metal–semiconductor (MS) interface has been a subject of extensive investigations for several years and the fundamental mechanisms that determine the barrier height are still not fully understood.[14–17] The interface properties of the MS contacts have a dominant influence on the device performance, reliability, and stability. Schottky barrier inhomogeneity at MS interfaces has been considered as an important factor in explaining the non-ideal behavior of the Schottky diodes. The Schottky contact's quality with a sufficient height barrier (Φ_b) and low leakage current are critical factors for the realization of the Schottky diode. In fact, the barrier height (Φ_b) is a key parameter of the junction, controlling both the width of the depletion region in the semiconductor and the electron current across the interface. The analysis of the current voltage (I–V) characteristics of the Schottky barrier diodes (SBDs) at room temperature does not only give detailed information about their conduction process or the nature of barrier formation at the MS interface.[18,19] But, the temperature dependence of the I–V characteristics allows us to understand different aspects of conduction mechanisms.[20–23] In this paper, the Schottky diode of Al/PVA:n-PbSe nanocomposite film has been fabricated. From I–V characteristics, parameters like series

[a]Author to whom correspondence should be addressed. Electronic addresses: surya@pu.ac.in and surya_tr@yahoo.com. Fax: +91-172-2783336. Tel.: +91-172-253622.

resistance (R_S), the ideality factor (n), the effective barrier height (Φ_b), the Richardson constant (A*), and the leakage current with the temperature have been calculated. The effect of temperature on the barrier height ($\Phi_{I\text{-}V}$) and ideality factor (n) is also studied. C-V measurements, in the reverse bias of Al/PVA:n-PbSe have been performed as a function of temperature and frequency and the values of barrier height ($\Phi_{C\text{-}V}$), the built-in–voltage (V_{bi}) and carrier concentration (N_D) and depletion layer width (W) have been calculated.

II. EXPERIMENTAL

Sodium selenosulphate (Na_2SeSO_3) has been chosen as the selenium source. Sodium selenosulphate aqueous solution (0.50 M) is prepared by adding 1.0 M of sodium sulfite in 50 ml of double de-ionized water, by adding 0.05 mol of selenium powder. The solution has been stirred for 7 h at 70 °C. The solution is kept overnight. Upon filtration, sodium selenosulfate solution is sealed and stored in the dark at 60 °C to prevent decomposition. PVA solution is obtained by adding 6.0 g PVA to 100 ml double de-ionized water and stirring at 60 °C until a viscous transparent solution is achieved. 0.1 M of metal sources, i.e., lead acetate has been dissolved in 20 ml of double de-ionized water. Ammonia or sodium hydroxide solution (2.0 M) is used to turn metal ions into complex ions and to reduce the free metal ion concentration. In a 50 ml flask, 20 ml PVA solution has been taken. Ammonia solution is then slowly added drop wise until a clear solution is obtained. After the *p*H value is adjusted with dilute acetic acid to about 10, 16.0 ml metal salt solution is added with constant stirring and 1 ml of selenosulphate solution is introduced in order to achieve the desired Pb: Se ratio. We have prepared the PVA:n-PbSe nanocomposites at different Pb:Se ratios, i.e.,1:1, 4:1, 8:1, and 16:1.The mixture is stirred for 6-7 h in room temperature to obtain a reddish brown color solution. The Al substrate is washed with NaOH or KOH pellets to remove native alumina layer and other soluble salts on the Al substrate. The PVA:n-PbSe material is deposited on Al substrate by casting method. Upon solvent evaporation, a PVA–selenide nanocomposite film has been obtained. The as-prepared film is finally washed with double de-ionized water to remove any soluble salts and kept for drying.

For device fabrication, an ohmic contact is defined as a metal-semiconductor contact that has a negligible contact resistance relative to the bulk or series resistance of the semiconductor. A satisfactory ohmic contact should not significantly degrade device performance and can pass the required current with a voltage drop that is small compared with the drop across the active region of the device. A Schottky barrier refers to a metal-semiconductor contact having a large barrier and low doping concentration that is less than the density of states in the conduction band or valence band. The Schottky junction Al/PVA:n-PbSe has prepared using a proper masking arrangement so as to form a square type device having an active area of 1 cm^2. The aluminum metal film about 1000 A thickness has been deposited by direct evaporation on PVA:n-PbSe films. The area of the diode is 3.2×10^{-3} cm^2. The vacuum of the order of 10^{-4} Pa is maintained during the evaporation. The schematic diagram of the fabricated Schottky diode is shown in Fig. 1. Transmission electron microscopy (TEM) has been done using the Hitachi H7500 electron microscope, operating at 90 kV. FTIR spectra have been recorded using the Perkin-Elmer PE-RX 1 FTIR spectrophotometer. The spectral resolution of the IR spectrophotometer is 1 cm^{-1}. Samples are prepared by putting the PVA:n-PbSe onto KBr pellet. Samples are prepared by putting the solution of PVA:n-PbSe nanocrystals onto carbon grids. The temperature dependence I–V measurements are taken with Keithley's electrometer from 273 to 333 K. The C-V measurements are taken with the Hioki 3532-50 LCR Hi-Tester, at a frequency range of 100 Hz-50 kHz and at temperature range of 283-333 K.

III. RESULTS AND DISCUSSION

A. Transmission electron microscope

Transmission electron microscopy (TEM) provides information regarding morphology and size distribution of selenide particles. Figure 2 depicts a TEM micrograph of the as-prepared PVA–composite. The well dispersed single nanorods of PbSe have an average diameter of 17.5 nm. There is no clamping of PVA and PbSe. Lead selenide nanorods are homogenously dispersed in PVA. We have prepared the PVA:n-PbSe nanocomposite at different Pb:Se ratios of 1:1, 4:1, 8:1, and 16:1 with an average diameter of 80, 50, 23, and 17.5 nm. The optical bandgap of these ratios as obtained from the UV/VIS spectra is 1.48, 1.49, 1.51, and 1.6 eV. The larger bandgap and smaller particle size at Pb:Se:16:1 suggests that it is highly quantum confined as compared to other ratios. Therefore, we have decided to study the PbSe-PVA nanocomposite films in the Pb:Se:16:1 ratio in detail.

B. FTIR spectroscopy

To investigate the interaction between the PbSe nanorods and the PVA matrix, the infrared spectra has been measured. Figures 3(a) and 3(b) show the FT-IR spectra of pure PVA film and PVA:n-PbSe nanocomposite film. The FTIR spectra of these films show that there is a good chemical bonding between PVA and PbSe. We observe a band at 3419 cm^{-1}, which can be assigned to the asymmetric stretching vibration of O-H. It shows a large downshift in the spectra of PVA: n-PbSe. This is due to the weakening of the O-H bond when PVA binds to PbSe nanorods. In the FTIR spectrum of pure PVA, the band at $\nu \sim 2143.2$ cm^{-1} is due to C-H wagging

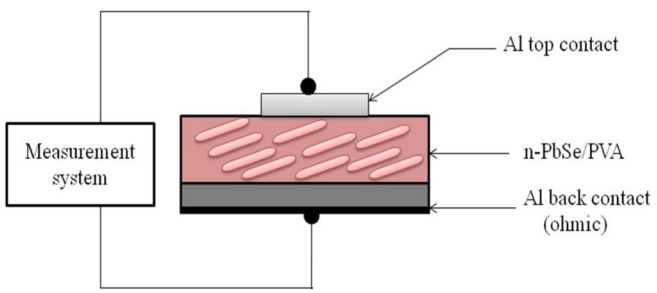

FIG. 1. Diode structure.

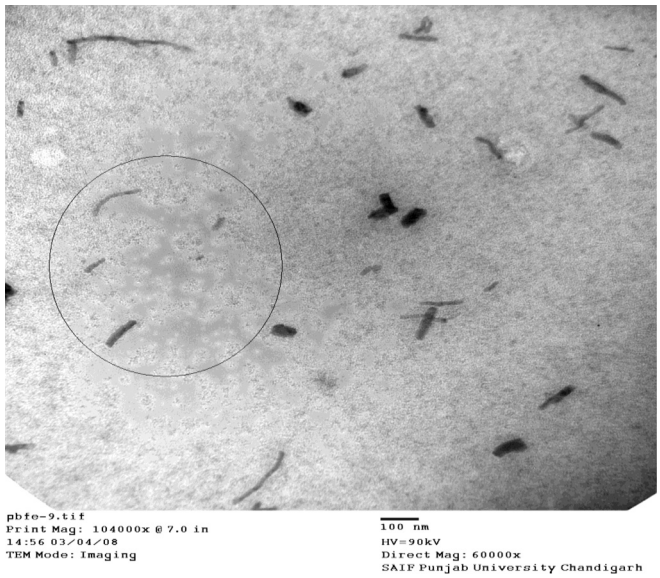

FIG. 2. TEM image of the polymer embedded PbSe nanorods.

vibrations. The absorption bands occurring at 1643 cm^{-1} and 1419 cm^{-1} is due to C=C stretching bands and bending vibrations of CH_2 groups, respectively. The stretching band at 1150 cm^{-1} is known to be the crystallization-sensitive band of PVA and is taken as a measure of the degree of crystallinity. In addition, the 1150 cm^{-1} band inferred that it might be due to a kind of absorption mechanism related to the presence of an oxygen atom. The band at about 1095 cm^{-1} is assigned to the Se-H bond showing an interaction between PVA and PbSe. The FTIR spectrum of the PVA:n-PbSe nanocomposite shows a decrease in the transmittance of the band at $\nu \sim 1406\,cm^{-1}$, in comparison with the band at $\nu \sim 1419\,cm^{-1}$, which indicates the decoupling between O-H and C-H vibrations due to the bonding interaction between O-H and PbSe nanorods. The bands at $\nu \sim 687.6\ cm^{-1}$ indicate the out-of-plane vibrations of O-H and C-H in the PVA spectra.

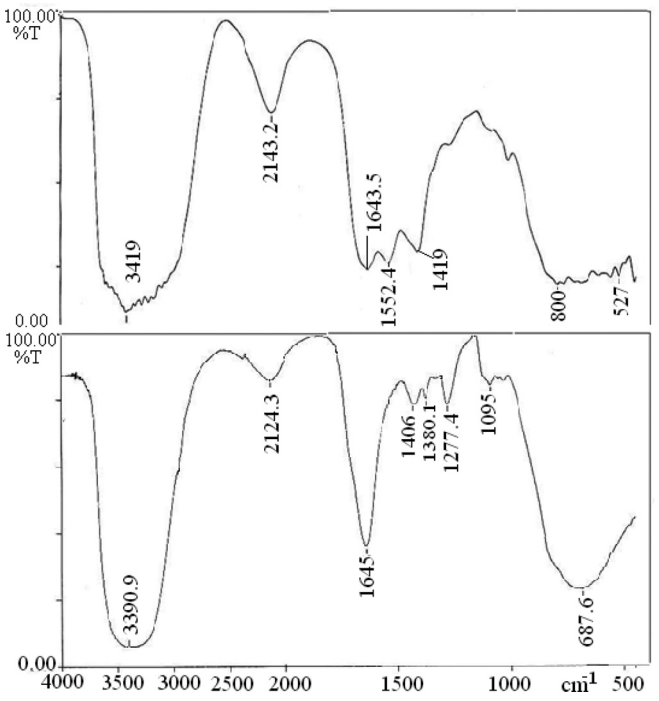

FIG. 3. FTIR spectra of (a) PVA and (b) PVA:n-PbSe.

C. Temperature dependent forward current-voltage (I-V) characteristics

The current-voltage characteristics for the Schottky diode[24] are as follows:

$$I = I_S\left(\frac{qV}{nkT}\right)\left\{1 - \exp\left(\frac{qV}{nkT}\right)\right\}, \tag{1}$$

$$I_s = AA^*T^2\exp\left(\frac{-q\Phi_b}{kT}\right), \tag{2}$$

where, I is current flowing, I_s the saturation current density, n is the ideality factor, A is diode area, A^* is the Richardson constant, where $m^* = 0.07m_0$,[25] T is the absolute temperature, ϕ_b is the Schottky barrier height, and k is the Boltzmann constant (8.62×10^{-5} eV/k). This method fails when the influence of the series resistance is already significant at medium or small forward voltages or even at reverse bias. Another conduction mechanism such as generation–-recombination current or leakage current is also taken into account to explain the nonideality of the curves. When a metal–semiconductor (MS) structure with the R_s is considered, according to the TE theory, it is assumed that the relation between the applied forward bias voltage V, and the current I is expressed as

$$I = I_S\left(\frac{q(V - IR_S)}{nkT}\right)\left\{1 - \exp\left(\frac{q(V - IR_S)}{kT}\right)\right\}, \tag{3}$$

where I_0 is the reverse saturation current derived from the straight line intercept of the current zero bias, and is given by

$$I_s = AA^*T^2\exp\left(\frac{-q\Phi_b}{kT}\right). \tag{4}$$

From equations (3) and (4), the barrier height (Φ_b) and ideality factor (n) of the Schottky diode is calculated from the following relation:

$$\Phi_b = \left(\frac{kT}{e}\right)\ln\left(\frac{AA^*T^2}{I_s}\right), \tag{5}$$

$$\frac{1}{\eta} = \frac{kT}{q}\frac{d(V)}{d(\ln I)}. \tag{6}$$

Figure 4 shows the semi logarithmic forward current-voltage characteristics of the Al/PVA:n-PbSe Schottky diode at temperature range 273-333 K. I-V characteristics of Al/PVA:n-PbSe show an appreciable increase in the forward bias conditions. This shows good diode characteristics. By extrapolating the values of current density to zero voltage axis gives the saturation current. The barrier height and ideality factor is obtained from the slope and intercept of this graph of the linear region of the forward-bias ln(I)

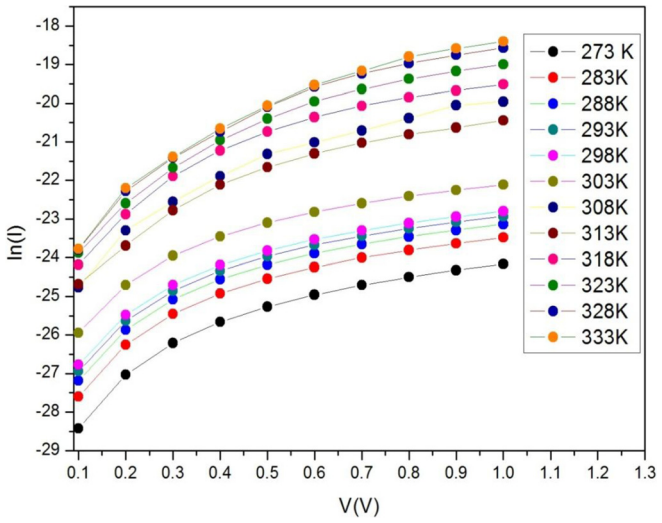

FIG. 4. Al/PVA:n-PbSe Schottky diode ln I vs V curves at different temperatures.

versus V plot at each temperature by using equations (5) and (6). The Schottky barrier height φ_b and ideality factor is found to be 0.89 eV and 1.9 at 273 K. The diode shows a large ideality factor. There may be a portion of the device nonideality attributable to generation recombination currents due to deep levels in PbSe. However, tunneling mechanisms probably provide a greater contribution to both the high device currents and device nonideality. Another possibility for the high leakage current is due to the oxide layer on the PbSe, even though the removal of the oxide layer during Schottky diode fabrication has been conducted, the exposure from the atmosphere was unavoided resulting in a native oxide on the PbSe surface. The oxide layer degraded the rectifying properties of metal contact deposited on the surface. The greater value of the ideality factor is caused by the interfacial layer and surface states.[26]

D. Zero-bias barrier height

Figure 5 shows the plot of temperature dependence barrier height and ideality factor for the Al/PVA:n-PbSe Schottky diode in the temperature range 273-333 K. As seen from the figure, while the ideality factor decreases almost exponentially, the barrier height increases linearly with the temperature. Thus, the experimental values of n [Fig. 5] decrease with the increase in temperature, and are all greater than one indicating that the thermionic emission is not the dominant conduction mechanism, but it is rather a tunneling mechanism assisted by traps at the metal/semiconductor interface. The barrier height values increase with temperature, as can be seen in Fig. 5. The current transport across the MS interface is a temperature-activated process.[27–30] Electrons at low temperatures are able to surmount the lower barriers and so transport mechanism will be dominated by current flowing through the patches of lower Schottky barrier height. As the temperature increases, more and more electrons gain sufficient energy to surmount the higher barrier. As a result, the dominant barrier height will increase with the temperature and bias voltage.[31,32] In general, the barrier height and built-in voltage should not exceed than the bandgap of particular materials. PVA:n-PbSe nanocomposites have a bandgap of 1.6 eV as obtained from UV/VIS spectra which is larger than the bandgap ($E_g = 0.27$ eV) due to quantum confinement effect in PbSe nanorods, so the barrier height and built-in voltage does not exceed bandgap ($E_g = 1.6$ eV).

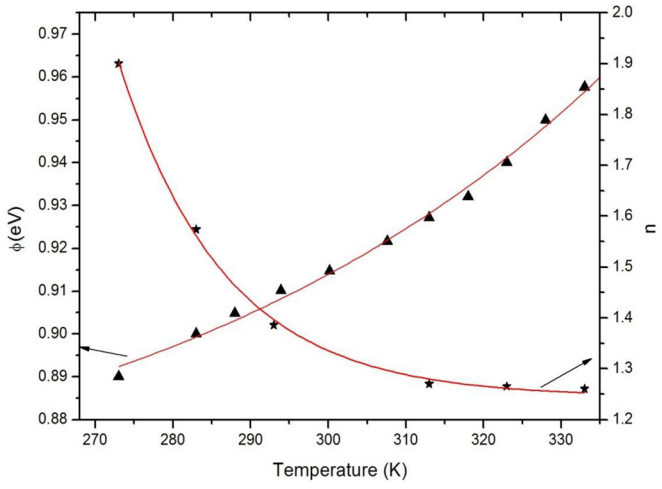

FIG. 5. Temperature dependence of the barrier height and ideality factor for the Al/PVA:n-PbSe Schottky diode.

E. Richardson plot

To determine the barrier height in a different way, we use the Richardson plot of the reverse saturation current I_0. By taking the natural logarithm of equation (4), equation can be rewritten as

$$ln\left(\frac{I_0}{T^2}\right) = \ln(AA^*) - \frac{q\Phi_b}{kT}. \quad (7)$$

Figure 6 shows the conventional energy variation of ln (I_0/T^2) against 1000/T. The dependence of ln(I_0/T^2) versus 1000/T is found to be nonlinear. In addition, it is impossible

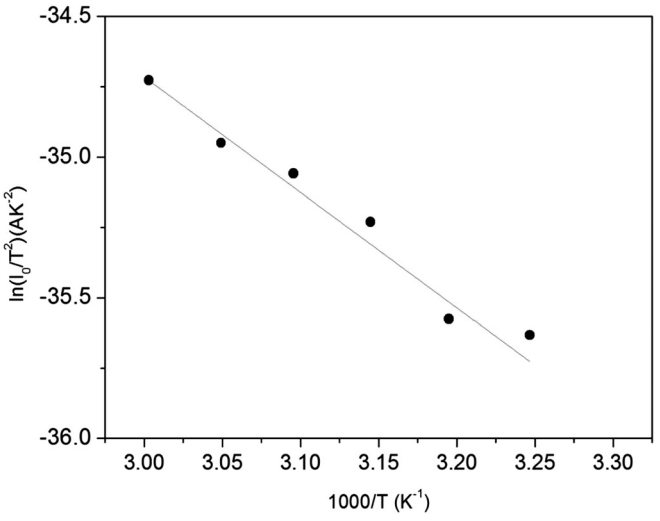

FIG. 6. Richardson plots of ln (I_0/T^2) vs $10^3/T$ for Al/PVA:n-PbSe Schottky diode.

to fit the experimental data. The experimental data are shown to fit asymptotically with a straight line at higher temperatures only. The value of the Richardson constant is 5.72×10^{-8} A cm^{-2} K^{-2} and mean activation energy (Φ_b^*) is equal to 0.14 eV.

This value is lower than the known value of Richardson constant 9.1 A cm^{-2} K^{-2}. The deviation in the Richardson plots may be due to the spatial inhomogeneous barrier heights and potential fluctuations at the interface that consist of low and high barrier areas. In other words, the current of the diode will flow preferentially through the lower barriers in the potential distribution. The value of the Richardson constant is affected by the lateral inhomogeneity of the barrier[33] and it is different from the theoretical value.

F. Effect of series resistance (R_s)

R_s is an important parameter particularly in the downward curvature of the forward bias *I–V* characteristics at a sufficient bias voltage. The presence of R_s in the structure added to the resistance of the epitaxial layer is responsible for the deviation of characteristics from linearity. In this case, to determine the φ_b, n, and R_s, Cheung's function method can be used.[34] According to Cheung's function method, equation (8) can be expressed as

$$\frac{dV}{d(lnI)} = IR_s + \frac{nkT}{q} \tag{8}$$

and

$$H(I) = V + \frac{nkT}{q}\ln\left(\frac{I}{AA^*T^2}\right) = IR_S + n\Phi_{eff}. \tag{9}$$

Equation (8) should give a straight line for the data of the forward-bias *I–V* characteristics. Thus, the slope and *y*-axis intercept of the d*V*/d(ln *I*) versus *I* plot will give R_s and nkT/q, respectively as shown in Fig. 7. The plots associated with these functions are given in Fig. 7. The value of n has been determined using equation (8) and found to be ~1.583. The temperature dependence of ideality factor with temperature are shown in Fig. 5. Figure 8 shows a plot of $H(I)$ versus I according to equation (9) will also give a straight line with the *y*-axis intercept equal to $n\Phi_b$. The slope of this plot also provides a second determination of R_s that can be used to check the consistency of Cheung's approach. From equation (8) according to the d*V*/d(ln *I*) versus *I* plot, the values of 19.65 MΩ and 1.581 for R_s and the ideality factor n of the device were obtained, respectively. The values of 20.39 MΩ and 0.837 eV for R_s and Φ_b were also obtained from *H*(*I*)–*I* plots, respectively. The R_s values obtained from both plots are in close agreement with each other as shown in Fig. 9. As seen in the figure, the R_s calculated from the Cheung function shows an unusual behavior that it increases with an increase of temperature. Such temperature dependence is an obvious disagreement with the reported negative temperature coefficient of the R_s. The series resistance increases with increasing temperature as could be expected for semiconductors in the temperature region where there is no carrier freezing out which is non-negligible only at low temperatures. Similar temperature dependence was obtained experimentally[35,36] and theoretically.[37]

The Cheung-Cheung plots (H(I)-I and dV/dln(I)-I) seems unusual that could be expected from any Schottky diode behavior is due to presence of the polymer layer. The obtained series resistance is higher due to the PVA polymer which has the low mobility and electrical conductivity with respect to PbSe semiconductor. Gökçen *et al.*[38] has reported an effect of PVA on the series resistance of SBDs. They have calculated the value of the series resistance for the metal-polymer-semiconductor (MPS) diode and metal-semiconductor (MS) diode. The value of series resistance calculated for the MPS diode is more than the MS diode which is due to effect that PVA polymeric composite layer generates a physical barrier between the metal and semiconductor.[38] Similar results are shown by other researchers also on semiconductor material with a layer of different polymer[39] and dye organic materials.[40]

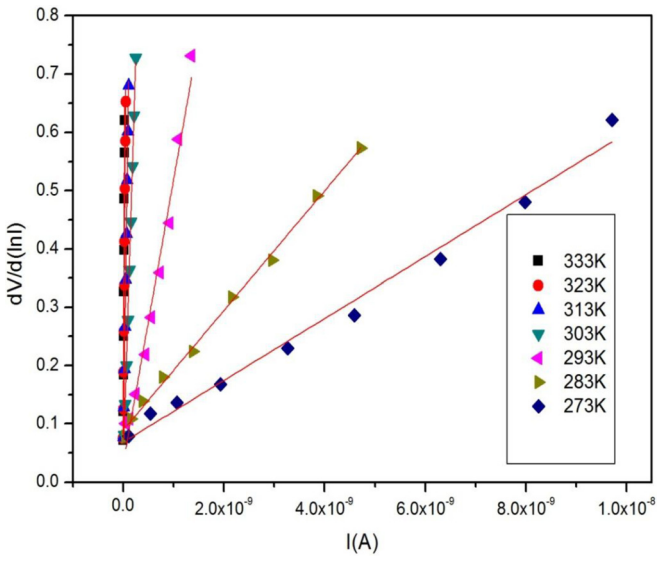

FIG. 7. Temperature dependence plot of d*V*/d(ln *I*) vs *I* for the Al/PVA:n-PbSe Schottky diode.

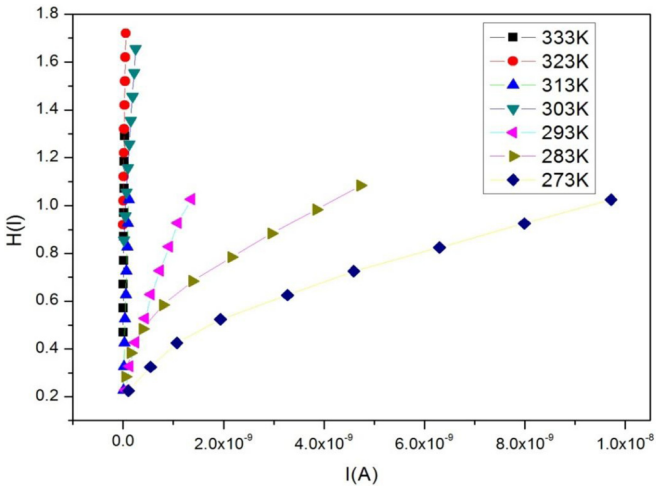

FIG. 8. Temperature dependence plot of H(*I*) vs *I* for the Al/PVA:n-PbSe Schottky diode.

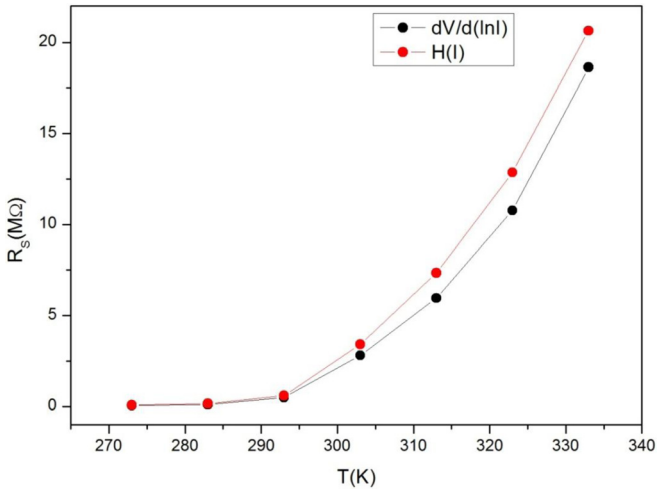

FIG. 9. Temperature dependence of the series resistance for the Al/PVA:n-PbSe Schottky diode.

G. Reverse current–voltage characteristics

Figure 10 shows the reverse bias semi-logarithmic I-V characteristics (up to −1.5 V) for this diode at various temperatures. For V = −1 V, the measured leakage current of the Al/PVA:n-PbSe Schottky barrier diode is 2.36×10^{-9} A at 273 K while it is 3.6×10^{-7} A at 333 K as shown in Fig. 11. The increase of the leakage current with temperature is due to the tunneling through the surface and bulk states. The tunneling mechanism in PVA:n-PbSe is assisted by some interface states such as dislocations and possibly oxygen vacancies in polyvinyl alcohol.[41,42] This mechanism has already been proven based on the ideality factors extracted from the forward I-V-T plots.

H. C-V measurements

In order to study nature of depletion region in the Schottky barrier, C-V characteristics are studied.[43] The mode of measurement depends on the capacitance, when

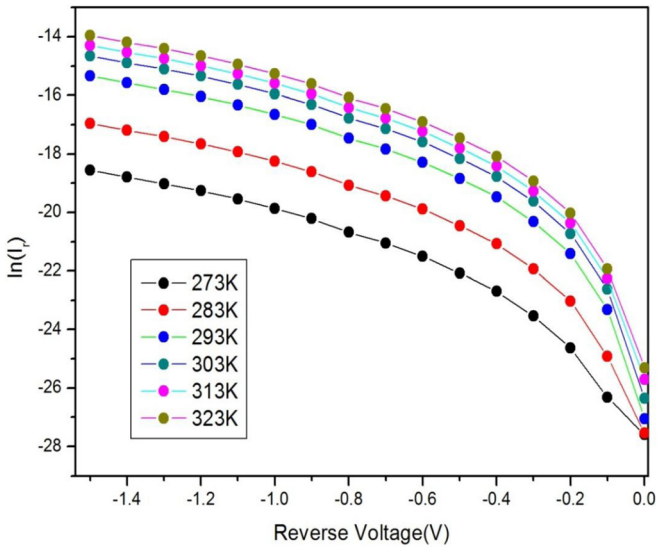

FIG. 10. Reverse-bias I-V characteristics of the Al/PVA:n-PbSe Schottky diode at various temperatures.

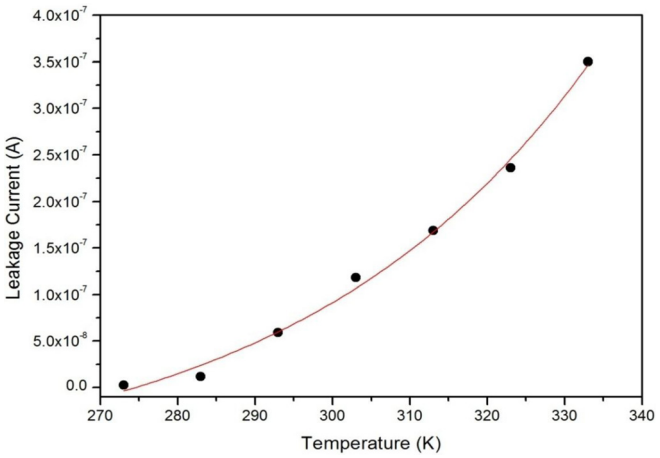

FIG. 11. Variation of leakage current with voltage.

the element is reverse biased. Under the reverse-bias conditions, there is a region of uncovered charge on either side of the junction that together makeup the depletion region and define the depletion width W. As the reverse-bias potential increases, the width of the depletion region increases, which in turn reduces the capacitance.[44] The depletion-layer capacitance C can be given by the equation

$$C = \left|\frac{dQ_{sc}}{dV}\right| = \sqrt{\frac{q\varepsilon_S A^2 N_D}{2(V_{bi}+V)}} = \frac{\varepsilon_S}{W} \tag{10}$$

and

$$\frac{1}{C^2} = \frac{2(V_{bi}-V)}{q\varepsilon_S A^2 N_D}. \tag{11}$$

Figure 12 shows the plot of $1/C^2$ versus reverse bias voltage at different temperatures of Al/PVA:n-PbSe Schottky diode at constant frequency 100 kHz. All the plots satisfy the linear relation. The depletion-layer width W is obtained from equation (10),

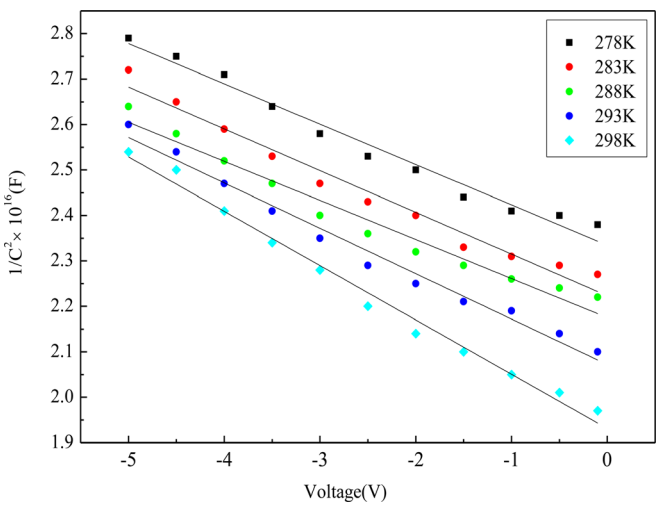

FIG. 12. Temperature dependence of the capacitance vs reverse voltage for the Al/PVA:n-PbSe Schottky diode.

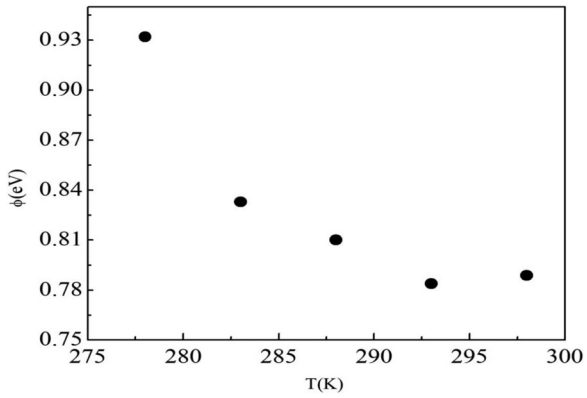

FIG. 13. Temperature dependence of the barrier height for the Al/PVA:n-PbSe Schottky diode.

$$W = \sqrt{\frac{2\varepsilon_S(V_{bi}+V)}{qN_DA^2}}. \quad (12)$$

From the intercept and slope of the graph, the built-in voltage and carrier concentration is calculated. The carrier concentration is obtained by the following equation:

$$N_D = \frac{2}{q\varepsilon_S A^2}\left[-\frac{1}{d(1/C^2)/dV}\right]. \quad (13)$$

As the barrier height is the sum of the built-in voltage V_{bi} and V_n, the V_n can be calculated from the equation

$$V_n = \frac{kT}{q}\ln\left(\frac{N_C}{N_D}\right) = 0.0259\ln\left(\frac{N_C}{N_D}\right), \quad (14)$$

where $N_C = 2(2\pi mkT/h^2)^{3/2}$ is acceptor concentration and N_D is the donor concentration. The value of the built-in-voltage, barrier height, carrier concentration, and depletion layer width at 278 K is found to be 0.40 V, 0.93 eV, 6.74×10^{16} cm^{-3}, and 3.22×10^{-5} cm, respectively.

I. Temperature dependent C-V measurement

Figure 13 shows the plot of the temperature dependence barrier height for the Al/PVA:n-PbSe Schottky diode in the temperature range of 278-301 K. It is found that the barrier height of the Schottky diode decreases with an increase in temperature. The temperature dependence parameters like built-in-voltage, carrier concentration, and depletion-layer width are calculated from equations (12), (13), and (14) is shown in Table I.

Figure 14 shows the dependence of capacitance C on frequency f at various temperatures. The capacitance decreases with increasing frequency. A wide dispersion in the capacitance values is observed at lower frequencies. However, at the lowest temperature of 303 K, the capacitance decreases only very slightly with frequency. At higher frequencies the curves for all temperatures tend to a common capacitance value. A decrease in capacitance with increasing frequency has been observed in several other materials, like CdSe.[45]

Figure 15 shows the variation of capacitance with temperature in the frequency regime 100 Hz-50 kHz. Figure 15

TABLE I. Parameters obtained from the temperature dependent C-V measurement.

Temperature	Barrier height (eV)	Built-in-voltage (V)	Carrier-concentration (cm^{-3})	Depletion- layer width (cm)
278 K	0.93	0.40	6.74×10^{15}	3.22×10^{-5}
283 K	0.83	0.30	6.52×10^{15}	2.58×10^{-5}
288 K	0.81	0.30	6.96×10^{15}	2.51×10^{-5}
293 K	0.78	0.25	6.05×10^{15}	2.23×10^{-5}
298 K	0.79	0.25	4.90×10^{15}	1.80×10^{-5}
301 K	0.71	0.20	4.60×10^{15}	1.82×10^{-5}

shows at lower temperatures, the capacitance is very sensitive to frequency, but at higher temperatures, the curves characteristic of the individual frequencies are well separated. This type of behavior has been previously accounted for in terms of the equivalent circuit model of Goswami and Goswami.[46] According to this model each capacitive system is assumed to be comprised of (1) an inherent frequency and temperature independent capacitive element C', (2) discrete temperature-dependent resistive element R due to the conducting film in parallel with C', (3) both elements in series with a constant low value resistance r due to lead lengths, etc.

According to this model, the measured series capacitance is given by

$$C = C + \frac{1}{\omega^2 R^2 C}. \quad (15)$$

The resistive element R is assumed to be thermally activated, with temperature variation is given by

$$R = R_0 \exp\left(\frac{\Delta E}{kT}\right), \quad (16)$$

where R_0 is a constant and ΔE is activation energy. Equation (15) predicts that measured capacitance should decrease with increasing frequency, but at higher frequencies becoming independent and reaching a constant value C'. For any

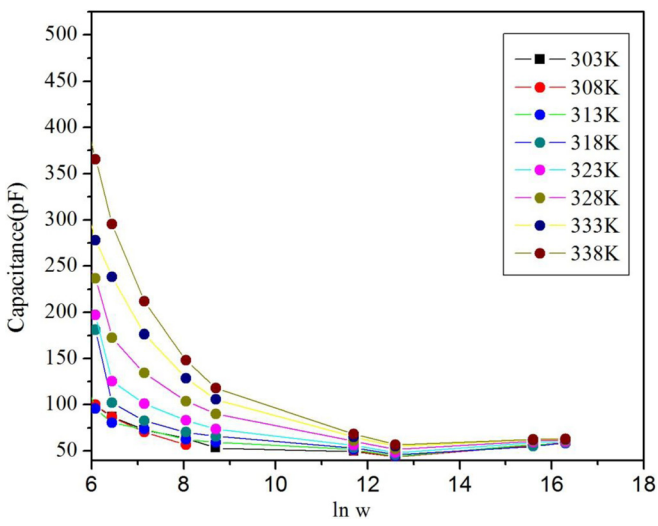

FIG. 14. Temperature dependence of capacitance vs frequency at different temperatures.

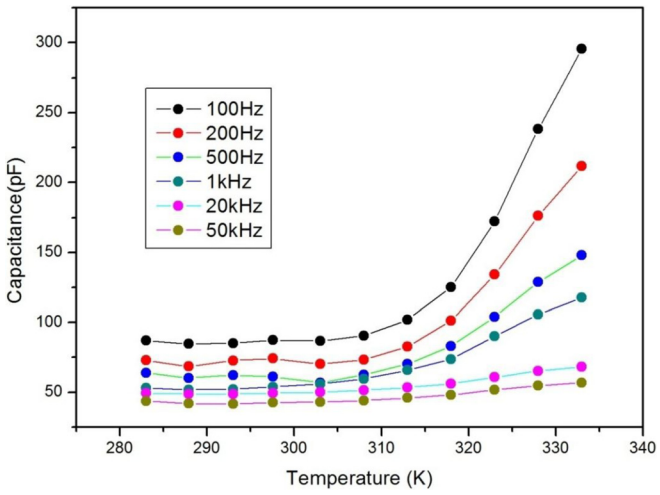

FIG. 15. Variation of capacitance with temperature at different frequencies.

particular frequency, the capacitance increases with increasing temperature. The resistive element R decreases with increasing temperature from Eq. (16). All of these effects are qualitatively equivalent in Figs. 14 and 15, where the value of C tends to a constant value at low temperature.

In general, a full treatment of Schottky barrier diodes results in a forward current equation of the form

$$I = ABT^2 \exp\left(\frac{-q\Phi_b}{kT}\right)\exp\left(\frac{-qV}{nkT}\right), \tag{17}$$

where B is a constant containing parameters of the junction properties and n is an ideality factor. The mathematics of this derivation is similar to that of thermionic emission, and the factor B corresponds to an effective Richardson constant in the thermionic problem. At thermal equilibrium, the current density is balanced by two equal and opposite flow of carriers, thus there is zero net currents. Electrons in the semiconductor tend to flow (or emit) into the metal, and there is an opposing balanced flow of electrons from metal into semiconductor. These current components are proportional to the density of electrons at the boundary,

$$|J_{m\to s}| = |J_{s\to m}| \infty \quad n_{th}, \tag{18}$$

$$|J_{m\to s}| = |J_{s\to m}| = C_1 N_C \exp\left(\frac{-q\Phi_b}{kT}\right), \tag{19}$$

where $J_{m\to s}$ is the current from the metal to semiconductor, $J_{s\to m}$ is current from semiconductor to metal.

Referring to Fig. 16, a semiconductor surface contains surface states due to incomplete covalent bonds and other effects, which can lead to charges at the metal semiconductor interface.[44] Because of the surface states, it is difficult to fabricate junctions with barriers near the ideal values predicted from the work functions of the two isolated materials. So, measured barrier heights are used in the device design. For example, a collection of interface states in the semiconductor bandgap that pin the Fermi level at a fixed position, regardless of the metal used. A collection of interface states located 0.7-0.9 eV below the conduction band pins E_f at the surface of n-type GaAs, and the Schottky barrier height is determined

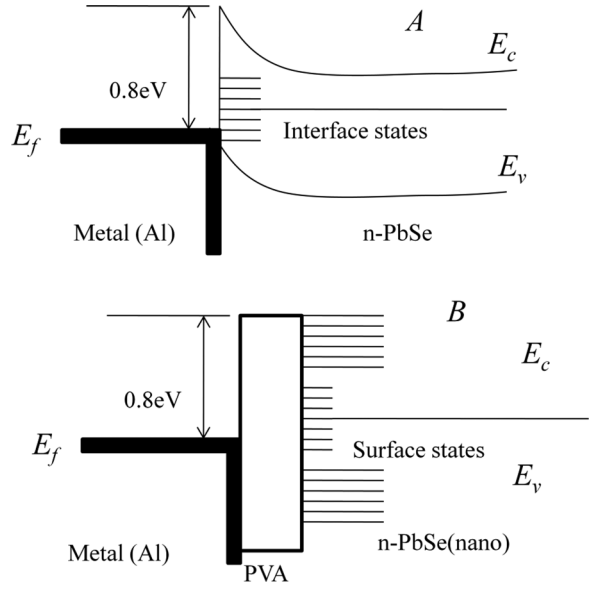

FIG. 16. Schematic of energy band profile for Al/bulk PbSe and Al/PVA:-nano-PbSe.

from this pinning effect rather than by the work function of the metal.[47]

The schematic energy-gap diagram for Al/n-PbSe ($E_g = 1.6$ eV) is shown in Fig. 16. Figures 16(A) and 16(B) represent profiles of Al/bulk-PbSe and Al/PVA:nano-PbSe. In addition to the existence of discrete energy levels, the uniqueness of the latter case is that the surface states are not in direct touch with the metal and thus permanently belong to nano-PbSe. Such states, where electrons are believed to be trapped, are made available to respond when one applies high signal frequency. In the ideal case, the discrete levels are supposed to be slanted due to biasing to facilitate carrier transport. Now when the frequency of recombination matches with the applied frequency, all the trap carriers are expected to be swept away. On the other hand, low frequency would have negligible or no effect upon the surface traps. But at higher frequency ranges, current transport due to the trap related mechanism becomes significant. Secondly, nano-PbSe possesses discrete energy levels (Fig. 16(B)) which could be slanted under proper biasing to facilitate current transport. Hence, it is evident that trapped carriers are basically frequency dependent where electron transport between slanted quantized levels through thin dielectric polymer depends on the biasing and temperature condition.[48]

J. Discrepancy between barrier heights

The forward bias current-voltage (I-V) and reverse bias capacitance-voltage (C-V) characteristics of the Al/PVA:n-PbSe Schottky diodes (SDs) are investigated over a wide range of temperature. The basic difference is in the biasing mode which makes barrier height increase in I-V measurement and decrease in C-V measurement. According to thermionic emission theory (TE) mechanism, the zero bias barrier height $\Phi_{I\text{-}V}$ calculated from I-V characteristics is found to increase with increasing temperature where biasing mode is forward biased. The increase of $\Phi_{I\text{-}V}$ with temperature is attributed to homogeneity of the Schottky barrier at the

metal-semiconductor interface. For an inhomogeneous barrier, the effective barrier height for thermionic emission increases with temperature due to the spreading of electric field distribution of charge carriers.[37] However, the barrier height determined from the C^{-2}-V characteristics at high frequency decreased linearly with increasing temperature where biasing mode is reverse biased. The barrier height extracted from C-V measurements, $\Phi_{C\text{-}V}$ is governed by depletion region thickness and this is less sensitive to small scale inhomogeneity.[49]

Moreover, the difference between the BHs measured from *I–V* and those from *C–V* in the metal/semiconductor is also evidence for the Schottky BH inhomogeneity. The reason for this discrepancy between the measured SBHs is clear. The current in the *I–V* measurement is dominated by the current which flows through the region of low SBH, and the measured *I–V* SBH is significantly lower than the weighted arithmetic average of the SBHs. On the other hand, the barrier height measured from the *C–V* or flatband is influenced by the distribution of charge at the depletion region boundary and this charge distribution follows the weighted arithmetic average of the SBHs. Therefore, the SBH determined from the zero-bias intercept assuming thermionic emission as a current transport mechanism is well below the *C–V* or flat-band-measured BH and the weighted arithmetic average of SBHs.

An ideality factor n > 1 has been ascribed to several effects:

(1) Interface states at a thin oxide between metal and semiconductor.[50]
(2) Tunneling currents in highly doped semiconductor.[51]
(3) Image force lowering of the Schottky barrier in the electric field at the interface.[52]
(4) Generation-recombination currents within the space region.[53]

These four models describe extreme cases of Schottky contacts and all of them have in common that they assume a spatially homogeneous, more or less automatically flat interface between metal and semiconductor. The potential fluctuation model in the study of diodes explains that the deformation of spatial barrier distribution on spatially inhomogeneous Schottky contacts is the cause of the difference in values of Φ_B determined by I-V and C-V measurements.

K. Effect of barrier inhomogeneities on Φ_b and n

The above discussed unusual contact behavior can be explained by using an analytical potential fluctuation model based on spatially inhomogeneous barrier heights at the interface.[31,54] Suppose that the distribution of the barrier heights is Gaussian character with a mean value Φ_b and standard deviation σ_s, which can be given as

$$P(\Phi_b) = \frac{1}{\sigma_S\sqrt{2\pi}}\exp\left(-\frac{(\Phi_b - \phi_b)^2}{2\sigma_s^2}\right), \tag{20}$$

where $1/\sigma_S\sqrt{2\pi}$ is the normalization constant of the Gaussian barrier-height distribution. The total current for any forward bias V is then given by

$$I(V) = \int_{\infty}^{-\infty} I(\Phi_b, V)P(\Phi_b)d\Phi, \tag{21}$$

$$I = I_S \exp\left[-\frac{q}{kT}\left(\bar{\Phi}_b - \frac{q\sigma_s^2}{2kT}\right)\right]\exp\left(\frac{q(V - IR_S)}{n_{ap}kT}\right)\left\{1 - \exp\left(\frac{q(V - IR_S)}{kT}\right)\right\}, \tag{22}$$

where

$$I_S = AA^*T^2\exp\left(\frac{-q\Phi_{ap}}{kT}\right), \tag{23}$$

where n_{ap} and Φ_{ap} are the apparent ideality factor and barrier height at zero bias, respectively, and the latter is given by

$$\Phi_{ap} = \bar{\Phi}_b(T = 0) - \frac{q\sigma_s^2}{2kT}. \tag{24}$$

In the ideal case ($n = 1$), the expression is obtained as

$$\left(\frac{1}{n} - 1\right) = \rho_2 - \frac{q\rho_3}{2kT}. \tag{25}$$

The temperature dependence of σ_s is usually small and thus can be neglected.[31] However, it is assumed that σ_s and Φ_b are linearly bias dependent on Gaussian parameters such that $\Phi_b = \Phi_{b0} + \rho_2 V$ and $\sigma_s = \sigma_{s0} + \rho_3 V$, where ρ_2 and ρ_3 are the voltage coefficients that may depend on temperature and they quantify the voltage deformation of the barrier height distribution.[55] It is obvious that the increase of zero bias barrier height is caused by the existence of the Gaussian distribution and the extent of influence is determined by the standard deviation itself. Also, the effect is particularly significant at low temperatures. On the other hand, the abnormal decrease of ideality factor occurs due to the variation of mean barrier height and standard deviation with bias, i.e., terms involving voltage coefficients ρ_2 and ρ_3. Fitting of the experimental data in equation (4) or (24) and in equation (3) gives Φ_{b0} and n_{ap} at zero-bias respectively which should obey equations (24) and (25). Thus, the plot of Φ_{ap} versus $1/2kT$ (Fig. 5) should be a straight line that gives $\Phi_{b0} = 1.26$ eV and $\sigma_{s0} = -0.017$ V from the intercept and slope, respectively. The lower value of σ_{s0} corresponds to more homogeneous BH. Clearly, the diode with the best rectifying performance presents the best barrier homogeneity with the lower value of the standard deviation. It was seen that the value of $\sigma_{s0} = -0.017$ V is small compared to the mean value of $\Phi_{b0} = 1.26$ eV, indicating the presence of less interface inhomogeneities.

Barrier inhomogeneities can occur as a result of inhomogeneities in the composition of the interfacial oxide layer thickness. The standard deviation is a measure of the barrier inhomogeneity. The lower value of σ_{s0} corresponds to a more homogeneous barrier height. Nevertheless, this inhomogeneity and potential fluctuation dramatically affect temperature *I–V* characteristics. The temperature dependence of the ideality factor can be understood on the basis of equation (25). Fitting showing the ideality factor n in Fig. 17 is a straight

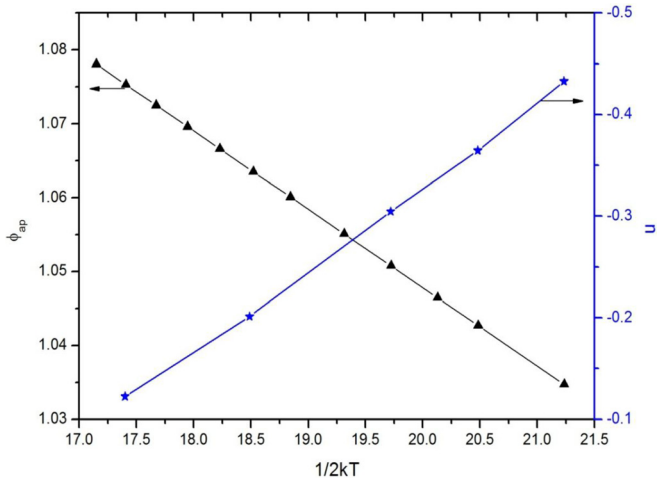

FIG. 17. Zero-bias apparent barrier height and ideality factor vs $1/T$ curves of the Al/PVA:n-PbSe Schottky diode according to Gaussian distribution of the barrier heights.

line that gives voltage coefficients ρ_2 and ρ_3 from the intercept and slope of the plot where $\rho_2 = 1.29$ and $\rho_3 = -0.08$ V from the experimental data. The linear behavior of the plot shows that the ideality factor expresses the voltage deformation of the Gaussian distribution of the SBD.

In general, the experimental values of n are greater than one indicating that the thermionic emission is not the dominant conduction mechanism, but it is rather a recombination-tunneling mechanism assisted by traps at the metal/semiconductor interface in the Al/PVA:n-PbSe Schottky diode. The Al/PVA:n-PbSe Schottky diode possesses some leakage current at reverse biasing due to a larger ideality factor. The barrier inhomogeneities also play an important role in explaining the transport properties of the metal-semiconductor contact of the Al/PVA:n-PbSe Schottky diode. These barrier height inhomogeneities that prevail at the interface behavior have been interpreted on the basis of the assumption of a Gaussian distribution of barrier heights using the potential fluctuation model.

IV. CONCLUSIONS

Polymer embedded nanorods formation of PbSe has been confirmed by TEM and FTIR spectra. The electrical properties like current-voltage, capacitance-voltage of Al/PVA:n-PbSe Schottky barrier diode is studied at wide range of temperatures. The temperature dependence of barrier height determined by I-V and C-V measurement is also studied. The effect of series resistance and leakage current at reverse bias is also considered to explain transport properties of Al/PVA: n-PbSe Schottky diode. The capacitance characteristics are studied at various temperatures and frequencies. The discrepancy of this barrier height is explained with the potential fluctuation model of barrier inhomogeneity at metal-semiconductor contact.

ACKNOWLEDGMENTS

This work is financially supported by DST (Major Research Project), N. Delhi. Ms. Mamta Sharma is thankful to UGC, N. Delhi for providing the fellowship.

[1]D. Y. Godovsky, Adv. Polym. Sci. **153**, 165 (2000).
[2]W. Caseri, Macromol. Rapid Commun. **21**, 705 (2000).
[3]R. B. Kale, D. Sartale, V. Ganesan, C. D. Lokhande, Yi-Feng Lin, and Shih-Yuan Lu, Appl. Surf. Sci. **253**, 930 (2006).
[4]K. Kellermann, D. Zimin, K. Alchalabi, P. Gasser, and H. Zogg, Physica E **20**, 536 (2004).
[5]D. Cui, J. Xu, S. Xu, G. Paradee, B. A. Lewis, and M. D. Gerhold, IEEE Trans. Nanotechnol. **5**, 562 (2006).
[6]J. M. Pietryga, R. D. Schaller, D. Werder, M. H. Stewart, V. I. Klimov, and J. A. Hollingsworth, J. Am. Chem. Soc. **126**, 11752 (2004).
[7]L. Qu and X. Peng, J. Am. Chem. Soc. **124**, 2049 (2002).
[8]W. Huynh, J. J. Dittmer, and A. P. Alivisatos, Science **295**, 225 (2002).
[9]P. S. Nair, K.P. Friz, and G. Scholes, Chem. Commun. **24**, 2084 (2004).
[10]I. Taçolu, U. Aydemir, E. Altındal, B. Knac, and S. Özçelik, J. Appl. Phys. **109**, 054502 (2011).
[11]I. Kang and F. W. Wise, J. Opt. Soc. Am. B **14**, 1633 (1997).
[12]M. Law, J. M. Luther, Q. Song, B. K. Hughes, C. L. Perkins, and A. J. Nozik, J. Am. Chem. Soc. **130**, 5974 (2008).
[13]R. K. Gupta and R. A Singh, Mater. Chem. Phys. **86**, 279 (2004).
[14]S. H. Huang, Y. Tian, and F. Lu, Appl. Surf. Sci. **234**, 362 (2004).
[15]M. M. Bülbül, S. Bengi, İ. Dökme, Ş. Altındal, and T. Tunç, J. Appl. Phys. **108**, 034517 (2010).
[16]Ö. F. Yüksel, M. Kuş, N. Şimşir, H. Şafak, M. Şahin, and E. Yenel, J. Appl. Phys. **110**, 024507 (2011).
[17]W. Mtangi, P. J. Janse van Rensburg, M. Diale, F. D. Auret, C. Nyamhere, J. M. Nel, and A. Chawanda, Mater. Sci. Eng. B **171**, 1 (2010).
[18]E. H. Rhoderick and R. H. Williams, *Metal–Semiconductor Contacts*, 2nd ed. (Clarendon, Oxford, 1988).
[19]R. T. Tung, Mater. Sci. Eng. R. **35**, 1 (2001).
[20]G. Liang, T. Cui, and K. Varahramyan, Solid-State Electron. **47**, 691 (2003).
[21]Ö. Güllü, M. Çankaya, M. Biber, and A. Türüt, J. Phys. Condens. Matter **20**, 215210 (2008).
[22]H. Cetin and E. Ayyildiz, Semicond. Sci. Technol. **20**, 625 (2005).
[23]S. Chand and S. Bala, Appl. Surf. Sci. **252**, 35 (2005).
[24]S. M. Sze, *Physics of Semiconductor Devices* 2nd ed. (Wiley, New York, 1981), p. 255.
[25]Landolt-Bornstein, *Group III Condensed Matter* (Springer-Verlag, Berlin, 1998), Vol. 41.
[26]G. Venkato Rao, G. Hema Chandra, O. M. Hussain, S. Uthanna, and B. Srinivasulu Naidu, Cryst. Res. Technol. **36**, 571 (2001).
[27]Ş. Karataş, Ş. Altındal, Solid State Electron. **49**, 1052 (2005).
[28]C. J. Panchal, M. S. Desai, V. A. Kheraj, K. J. Patel, and N. Padha, Semicond. Sci. Technol. **23**, 015003 (2008).
[29]M. K. Hudait, P. Venkateswarlu, and S. B. Krupanidhi, Solid State Electron. **45**, 133 (2001).
[30]B. Abay, G Çankaya, H. S. Güder, H Efeoğlu, and Y. K. Yoğurtç, Semicond. Sci. Technol. **18**, 75 (2003).
[31]S Chand, Semicond. Sci. Technol. **19**, 82 (2004).
[32]J. Osvald, Microelectron. Eng. **86**, 117 (2009).
[33]I. Dokme, S. Altindal, and M. Mahir Bulbul, Appl. Surf. Sci. **252**, 7749 (2006).
[34]S. K. Cheung and N. W. Cheung, Appl. Phys. Lett. **49**, 85 (1986).
[35]O. Pakma, N. Serin, T. Serin, and S. Altındal, Semicond. Sci. Technol. **23**, 105014 (2008).
[36]J. Osvald, Solid-State Commun. **138**, 39 (2006).
[37]J. Osvald and Zs. Horvath, Appl. Surf. Sci. **234**, 349 (2004).
[38]M. Gökçen, T. Tunç, S. Altındal, and I. Uslu, Current Appl. Phys. **12**, 525 (2012).
[39]F. Yakuphanoglu, Synth. Met. **160**, 1551 (2010).
[40]M. Shah, M. H. Sayyad, Kh. S. Karimov, and M. Maroof-Tahir, Physica B **405**, 1188 (2010).
[41]S. Saadaoui, M. M. B. Salem, M. Gassoumi, H. Maaref, and C. Gaquière, J. Appl. Phys. **110**, 013701 (2011).
[42]H. Kim, M. Schuette, H. Jung, J. Song, J. Lee, W. Lu, and J. C. Mabon, Appl. Phys. Lett. **89**, 053516 (2006).
[43]V. G. Bozhkov, N. A. Torkhov, and A. V. Shmargunov, J. Appl. Phys. **109**, 073714 (2011).
[44]C. Coskun, S. Aydogan, and H. Efeoglu, Semicond. Sci. Technol. **19**, 242 (2004).
[45]B. B. Ismail and R. D. Gould, Proc. SPIE **46**, 2780 (1996).
[46]A. Goswami and A. P. Goswami, Thin Solid Film **16**, 175 (1973).

[47]B. G. Streetman and S. Banerjee, *Solid State Electronic Devices* (Pearson Education Ltd. India, 2004), p. 226.
[48]D. Mohanta and A. Choudhury, J. Eur. Phys. B **45**, 63 (2005).
[49]V. G. Bozhkov, N. A. Torkhov, and A. V. Shmargunov, J. Appl. Phys. **109**, 073714 (2011).
[50]J. H. Werner, K. Ploog, and H. J. Queisser, Phys. Rev. Lett. **57**, 1080 (1986).
[51]R. F. Broom, H. P. Meir, and W. Walter, J. Appl. Phys. **60**, 1832 (1986).
[52]E. H. Rhoderick and R. H. Williams, *Metal Semiconductor Contacts*, 2nd ed. (Clarendon, Oxford, 1988), p. 118.
[53]J. H. Werner and H. H. Guuler, J. Appl. Phys. **69**, 1522 (1991).
[54]N. Tŭgluŏglu, S Karadeniz, M Şahin, and H Şafak, Semicond. Sci. Technol. **19**, 1092 (2004).
[55]A. F. Özdemir, A. Turut, and A. Kökçe, Semicond. Sci. Technol. **21**, 298 (2006).